

## OPTICAL COHERENCE TOMOGRAPHY FOR NONINVASIVE DIAGNOSIS OF EPITHELIAL CANCERS

Z. G. Wang<sup>1</sup>, C. Lee<sup>2</sup>, W. Waltzer<sup>2</sup>, Z. J. Yuan<sup>1</sup>, Z. L. Wu<sup>1</sup>, H. K. Xie<sup>3</sup>, Y. T. Pan<sup>1</sup>

<sup>1</sup>Department of Biomedical Engineering and <sup>2</sup>Department of Urology, State University of New York at Stony Brook, Stony Brook, NY 11794-8181;

<sup>3</sup>Dept of Electrical & Computer Engineering, University of Florida, Gainesville, FL 32611

*Abstract* — We summarize our recent progress in the development of the optical coherence tomography (OCT) systems suitable for clinical diagnosis and the preliminary results for *in vivo* diagnosis of epithelial cancers (e.g., bladder cancers). The endoscopic spectral-domain OCT system allows simultaneous, real-time, cross-sectional OCT images of tissue structure and functions (i.e., local Doppler blood flow) of biological tissue for enhanced diagnosis. A new approach to use spectral demodulation of elastic scattering is discussed for potential cancer grading. The transverse and axial resolutions of the OCT scopes are 12 $\mu$ m and 10 $\mu$ m, respectively. Results of the preliminary clinical studies show that unlike animal carcinogenesis models, bladder cancers in humans are more complicated in terms of epithelial backscattering changes: some lesions exhibit enhanced backscattering; some show reduced scattering owing to complex surface condition changes such as asperities or invaginations induced by tumorigenesis (e.g., papillary transitional cell cancers). Nevertheless, promising results can be provided by incorporating other diagnostic parameters such as changes in local vasculature and urothelial heterogeneity.

### 1. INTRODUCTION

Optical coherence tomography has been becoming an new enabling optical imaging technique that permits noninvasive or minimally invasive cross-sectional imaging of biological tissue at a resolution close to histopathology [1,

2]. Recent technological advances include ultrahigh-resolution OCT (uOCT) by utilizing ultra broadband source (e.g., ultrafast laser or Xe lamp) to image subcellular details of intact living cells [3], polarization-sensitive OCT to diagnose tissue birefringence [4], Doppler OCT to measure local blood flow [5], spectral-domain OCT to enhance imaging speed and image contrast and to detect tissue functions [6], and fluorescence-guided OCT for enhanced diagnosis [7]. In addition, various endoscopic OCT devices have been reported, which facilitated endoscopic laser scanning by a rotary fiberoptic joint connected to a orthogonal deflecting micro prism for circumferential scan [2] or by a small galvo plate to swing the distal fiber tip [8], or MEMS devices to steer laser beams [9-11], or a micro motor to rotate the OCT catheters for imaging different types of internal cavities such as flat surface or tubular surface. Interestingly, intense research in recent endoscopic OCT development has moved towards multi-modality imaging capability such as fluorescence guided OCT or OCT/Doppler OCT to explore physiological and functional diagnosis in addition to morphological modality, which has been found to show great promise. We will summarize our results in this area.

### 2. METHODS

The MEMS-based endoscopic OCT setups (both time domain OCT and spectral domain OCT) have been previously reported, therefore only a brief introduction is given here to highlight the technological improvement to

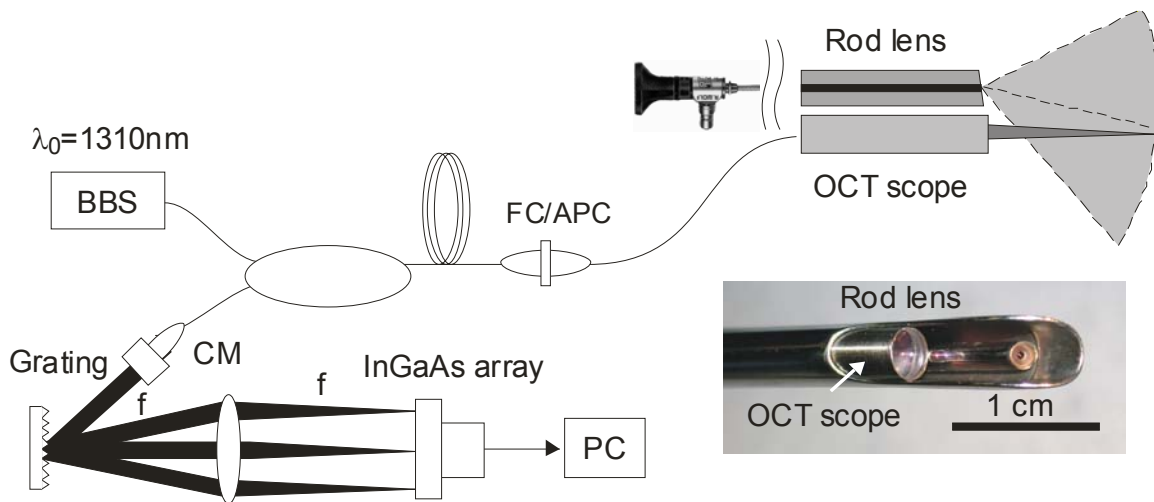


Fig.1 Schematic illustrating spectral domain (SD-OCT) setup to be connected to MEMS based OCT catheter for clinical diagnosis. A standard  $\phi 2.7\text{mm}$  hystoscope is used for visual guidance (white light or fluorescence). A  $\phi 5\text{mm}$  OCT scope is sealed onto the bridge to permit cross-sectional morphological and Doppler imaging of tissue.

enhance OCT image contrast and resolution as well as diagnostic efficacy and ease to handle in clinical settings. Major improvements are made on SD-OCT, including:

1) Removal of reference arm for phase stabilization. In this case, self interference instead of mutual interference is detected in SD-OCT, which simplifies fiber optics design and endoscopic packaging for reducing fluctuations induced by fiber bending and other unexpected effects in clinical setting.

2) Inclusion of a local beam splitter mirror in the endoscope as reference for stable phase retrieval and for reduction of stress-induced polarization (e.g., birefringence) fluctuation.

3) Simultaneous endoscopic OCT and Doppler OCT imaging at a frame rate of nearly 2-4 fps depending on image SNR.

A schematic of the endoscopic OCT imaging systems is depicted in Fig.1 which is based on a SD-OCT system illuminated by a broadband light source with pigtailed power of 19mW, central wavelength  $\lambda_0$  at 1310nm and spectral bandwidth  $\Delta\lambda_{\text{FWHM}}$  of 79nm (coherence length or axial resolution  $L_c=10\mu\text{m}$ ). Unlike previously reported SD-OCT setup which employed a stationary mirror in the reference arm of the fiberoptic Michelson interferometer,

to match the pathlength of the sample arm connected to the OCT scope inserted in the instrument channel of a 22Fr endoscope via an angled FC adaptor. Instead, we employ a beam splitter in the endoscope as a reference for interference detection. The light from the sample and reference mirror is recombined in the detection fiber, collimated by a f/55mm achromatic fiberoptic collimator, spectrally diffracted by a grating ( $d^{-1}=1200/\text{mm}$ ) and detected by a fast line InGaAs photodiode array (interpixel shift with 512 pixels) placed at the focal plane of a Fourier lens ( $f=120\text{mm}$ ). The spectral modulation induced by interference from different depth within tissue that corresponds to an A-scan in TD-OCT, is digitized via a 12-bit A/D at 5MHz and streamlined to the hard disk of an image workstation to permit full-size ( $1\text{k}\times 1\text{k}$ ) 2D OCT imaging at nearly 8fps. Doppler OCT is reconstructed with 2-3 repeating scans to retrieve the phase difference induced by blood flow in the submucosa and upper muscularis of bladder tissue, which can be displayed at 2-4 2fps depending on image SNR tolerance. The measured axial resolution is  $11\mu\text{m}$  (close to transform limit  $L_c\approx 10\mu\text{m}$ ), the lateral resolution is  $\sim 12\mu\text{m}$ . The system dynamic range is  $\sim 100\text{dB}$ , sufficient for bladder cancer diagnosis.

### 3. RESULTS

The CMOS-MEMS mirrors used in this study are 1.2mm×1.3mm in size and can thus support a  $\phi$ 1.1-1.2mm laser beam. The smooth scanning angle is  $28^\circ$  (optically) and the transverse 2D OCT image size is roughly 3.5mm. The self referenced OCT scope well tackles the challenge of path length mismatch due to patch core stretch in clinical diagnosis, so in most cases OCT imaging diagnosis can be completed in less than 10 minutes. The system is completely automatic, with on screen display of 2D OCT images and the corresponding Doppler OCT images. Histology is used as gold standard to evaluate OCT diagnosis.

Over 20 patients with over 50 lesions have been studied. Fig.2 shows the examples of the *in*

(TCC, stage Ta). Unlike those bladder cancers generated in animal models, there is no occurrence of the urothelial backscattering increase. However, unlike hyperplastic lesions either, the cancerous urothelium (U' as highlighted by a dashed circle) becomes highly heterogeneous because of hollow enclosures in the urothelium. For instance, at least 3 of such holes can be identified by OCT in panel 2b. Although we need more data to support the diagnosis, diagnosis of flat bladder cancers based on heterogeneity in the urothelium may be promising based on the accumulated cases. Panel 3 is a papillary TCC, which can be easily diagnosed even by surface image. The OCT image shows the transition from normal bladder to the cancerous lesions (U'' as highlighted by a dashed circle) with clear delineation. Similar to

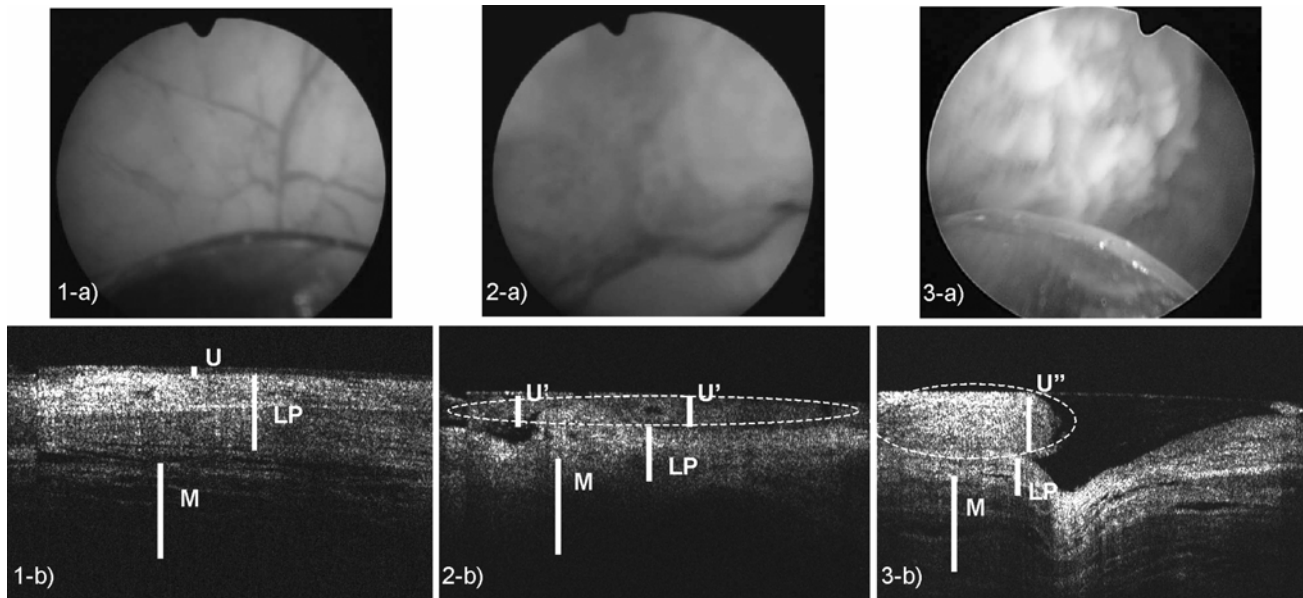


Fig.3 Spontaneous contractile waves and power spectra in a young rat bladder *ex vivo*. A) Time-lapsed 2D OCT; B) Power spectrum of the contractile waves at  $25.8^\circ\text{C}$ ; C) Power spectrum of the contractile waves at  $37.5^\circ\text{C}$ . A major difference is observed for the temperature dependence of the bladder contractility. The white arrows in panel (A) point to the contractile waves.

*vivo* results of endoscopic OCT diagnosis. Panel 1 (a: surface color image, b: OCT image) is a normal human bladder with clear delineation of the top thin layer of urothelium (U), followed a high scattering lamina propria (LP) and the upper muscularis layer. The normal urothelium is of low scattering and highly homogeneous. Panel 2 is a flat transitional cell carcinoma

animal models, the backscattering in the cancerous urothelium is enhanced drastically. As can be seen that even at the border of the papillary TCC, the underlying bladder morphology is very unclear, which implies the limitation of OCT to stage outgrowth bladder cancers. However, as indicated in Panel 1 and panel 2 that OCT can precisely determine the

boundary of bladder cancers, this technique can help urologists to precisely resect bladder tumors (TURBT).

#### 4. CONCLUSION

MEMS-based endoscopic SD-OCT can provide high-resolution cross-sectional images of bladder tissue morphological changes and diagnose diseases such as bladder cancers. *In vivo* human study has been conducted to examine the utility and potential limitations for future clinical applications and the preliminary results suggest that despite the complications of urothelial backscattering changes in cancerous lesions (either increase or decrease), endoscopic OCT, by analyzing urothelial heterogeneity and potentially local vascularization, has the potential to diagnose bladders including flat bladder cancers at a high sensitivity and specificity. It must be noted that staging of bladder cancer may be limited to Ta to T1 or T2a due to drastically decreased useful image depth in cancer areas. This work is partially support by NIH grants 2R01-DK059265 (YP) and R01-DK068401 (YP/WC).

#### 5. REFERENCES

1. Huang, D., et al., Optical Coherence Tomography. *Science*, 1991. **254**(5035): p. 1178-1181.
2. Tearney, G.J., et al., In vivo endoscopic optical biopsy with optical coherence tomography. *Science*, 1997. **276** (5321): p. 2037-2039.
3. Drexler, W., et al., In vivo ultrahigh-resolution optical coherence tomography. *Optics Letters*, 1999. **24**(17): p. 1221-1223.
4. deBoer, J. F., et al., Two-dimensional birefringence imaging in biological tissue by polarization-sensitive optical coherence tomography. *Optics Letters*, 1997. **22**(12): p. 934-936.
5. Chen, Z. P., et al., Noninvasive imaging of in vivo blood flow velocity using optical Doppler tomography. *Optics Letters*, 1997. **22**(14): p. 1119-1121.
6. Yun, S. H., et al., High-speed spectral-domain optical coherence tomography at 1.3  $\mu$ m wavelength. *Optics Express*, 2003. **11**(26): p. 3598-3604.
7. Pan, Y. T., et al., Enhancing early bladder cancer detection with fluorescence-guided endoscopic optical coherence tomography. *Optics Letters*, 2003. **28**(24): p. 2485-2487.
8. Zagaynova, E.V., et al., In vivo optical coherence tomography feasibility for bladder disease. *Journal Of Urology*, 2002. **167**(3): p. 1492-1496.
9. Pan, Y. T., H. K. Xie, and G. K. Fedder, Endoscopic optical coherence tomography based on a microelectromechanical mirror. *Optics Letters*, 2001. **26**(24): p. 1966-1968.
10. Herz, P. R., et al., Micromotor endoscope catheter for in vivo, ultrahigh-resolution optical coherence tomography. *Optics Letters*, 2004. **29**(19): p. 2261-2263.
11. Wang, Y. L., et al., Low-voltage polymer-based scanning cantilever for in vivo optical coherence tomography. *Optics Letters*, 2005. **30**(1): p. 53-55.
12. Pan, Y. T., Wang, Z. G. et al., High-resolution Optical Imaging Characterization of Bladder Dynamic Morphophysiology with Time-Lapse Optical Coherence Tomography, *Optics letters*, 2005 in press.